Received 15 June 2018; accepted 25 July 2018. Date of publication 15 August 2018; date of current version 27 August 2018.
The review of this paper was arranged by Editor C.-M. Zetterling.

Digital Object Identifier 10.1109/JEDS.2018.2860792

Electrothermal Evaluation of AlGaN/GaN Membrane High Electron Mobility Transistors by Transient Thermoreflectance

MARKO J. TADJER [1] (Senior Member, IEEE), PETER E. RAAD[4,5] (Senior Member, IEEE), PAVEL L. KOMAROV[5], KARL D. HOBART[1] (Member, IEEE), TATYANA I. FEYGELSON[2], ANDREW D. KOEHLER [1] (Member, IEEE), TRAVIS J. ANDERSON [1] (Senior Member, IEEE), ANINDYA NATH[3], BRADFORD PATE[2], AND FRITZ J. KUB[1] (Fellow, IEEE)

1 Electronics Science and Technology Division, U.S. Naval Research Laboratory, Washington, DC 20375, USA
2 Chemistry Division, U.S. Naval Research Laboratory, Washington, DC 20375, USA
3 GlobalFoundries, Inc., Hopewell Junction, NY 12533, USA
4 Department of Mechanical Engineering, Southern Methodist University, Dallas, TX 75205, USA
5 TMX Scientific, Richardson, TX 75081, USA

CORRESPONDING AUTHOR: M. J. TADJER (e-mail: marko.tadjer@nrl.navy.mil)

ABSTRACT A novel wet etch process for fabrication of large-area AlGaN/GaN membranes is reported, along with an evaluation of membrane-high electron mobility transistor (HEMT) electrothermal performance up to 1.9 W/mm. Hall measurements showed negligible post-etch change in membrane-HEMT sheet resistance, Hall mobility and carrier concentration. Static (dc) current-voltage characteristics showed negligible change in on resistance (R_{ON}), although $I_{DS,MAX}$ was significantly reduced due to increased self-heating in the absence of the Si substrate. Pulsed output characteristics were similarly affected as self-heating was expected to be still present at ms pulse widths. In the off state, the drain leakage current was measurably lower by about an order of magnitude. Pulsed-mode off-state step stress showed a dynamic on resistance improvement by about a factor of 2 when both sides of the membrane were passivated by SiN. A peak temperature of 148.5 °C was measured on the membrane HEMT using transient thermoreflectance imaging. These initial results indicate that substrate removal does not necessarily cause device degradation, and can be a promising step in improving HEMT reliability in future generations of power devices.

INDEX TERMS AlGaN/GaN, high electron mobility transistor, membrane, thermoreflectance imaging, current collapse, double-side passivation.

I. INTRODUCTION

AlGaN/GaN transistor devices have undergone rapid technological development in recent years and have emerged as a mature commercial platform for the development of high electron mobility transistors (HEMTs). Such transistors have found widespread commercial application in radio frequency (rf), and high power devices are being commercialized as well. Despite their commercial success based on the wide bandgap of GaN and high density two-dimensional electron gas formed near the AlGaN/GaN interface, heteroepitaxial AlGaN/GaN structures have a relatively high density of extended defects ($\sim 10^8$ $cm^{-2}$for GaN on Si). These dislocations form during growth as a result of the mismatch in lattice constant and coefficient of thermal expansion between the heterostructure and its substrate, despite being mitigated by an appropriately engineered III-Nitride nucleation layer [1]. While excellent GaN HEMT electrical performance has been reported over the years, such as high breakdown voltage and low current collapse, the long-term reliability of GaN is known to depend on thermal limitations, similarly to Si electronic devices. For the specific case of GaN-on-Si, the nucleation layers required for initiation of GaN heteroepitaxial growth, typically consisting of $Al_xGa_{1-x}N$ and AlN with even higher degree of density of defects, introduce an undesirable thermal boundary resistance which exacerbates self-heating effects and thus

limit AlGaN/GaN HEMT reliability [2]. As a result, there has been intensive research to improve the electrothermal performance of GaN-on-Si. Reports of improved thermal management have proposed the integration of high thermal conductivity layers such as diamond into HEMT fabrication process [3]. Anderson *et al.* [4] have shown that mid-process diamond improves not only the thermal, but also the electrical performance. Many other groups have also demonstrated that removing or replacing the (111) Si substrate can dramatically improve breakdown voltage and power performance [5]–[7]. Despite these encouraging results, a strained heteroepitaxial heterostructure such as AlGaN/GaN, whose mechanism of operation relies on piezoelectric polarization, would exhibit degraded performance without the mechanical support of a substrate in the immediate vicinity of the transistor active area. For example, Azize has demonstrated that blanket etching of the Si substrate could cause cracks in the AlGaN/GaN surface and while such degradation is less severe when room-temperature polishing is employed, strain mechanics dictates that it is not possible to produce a free-standing AlGaN/GaN membrane without mechanical support [8], [9]. Indeed, AlGaN/GaN nanomembrane HEMT devices where the substrate was removed only in the immediate vicinity of the channel have been reported by several groups. Herbecq *et al.* utilized a dry etch process for localized Si substrate removal, whereas Lu and Palacios developed a substrate transfer process where the entire substrate was replaced with quartz [6], [7]. Substrate removal by dry etching has also allowed the demonstration of small-area nanomembrane structures for capacitive and pressure sensor applications, as well as novel die transfer processes for flexible device applications [10]–[15]. Our work, on the other hand, has employed a novel process based on a well-known wet etchant for Si (HNA) to produce large-area, AlGaN/GaN HEMT membranes which do not exhibit additional tensile stress [16]. This approach has allowed us to effectively decouple the thermal contribution of the Si substrate when characterizing the electrothermal HEMT performance and isolate the intrinsic thermal performance of an AlGaN/GaN heterostructure where a high current density channel is capable of generating sufficient heat flux to render the GaN film thermally unstable and prone to decomposition under high temperature, high field operating conditions [17]. While severe degradation in HEMT performance is typically expected in this case, our work quantifies the HEMT characteristics that degrade and shows that an AlGaN/GaN membrane HEMTs can exhibit several key improvements at low power when compared to a conventional HEMT-on-Si. As a part of our study, we also report transient thermal performance of AlGaN/GaN HEMTs on Si for the first time, to the best of our knowledge, despite a number of time-resolved thermal studies of AlGaN/GaN HEMTs on sapphire and SiC substrates, as well as a transient electrical method for thermal characterization of GaN-based HEMTs on Si [18]–[21].

II. EXPERIMENTAL DETAILS

High electron mobility transistors (HEMTs) were fabricated on 2 nm GaN/17.5 nm $Al_{0.26}Ga_{0.74}N$/GaN heterostructures (1.9 μm total epilayer thickness) grown on a (111) oriented Si substrate utilizing standard processing techniques (Cl/Ar plasma mesa etch, rapid-thermal annealed Ti/Al/Ni/Au Ohmic contacts, Ni/Au gate, 100 nm PECVD SiN passivation, $L_G = 3$ μm, $L_{GD} = 10$ μm, $W_G = 75$ μm). The Si substrate was then etched in an HNA ($HF/HNO_3/CH_3COOH$) solution at room temperature using a custom spin/remove process aimed at producing several-mm wide circular AlGaN/GaN membranes, allowing the fabrication HEMTs with and without substrate on the same die (Fig. 1) [22]. A 100 nm thick PECVD SiN film was also deposited on the exposed N-polar side of the III-Nitride nucleation layers, effectively creating a double-side passivated HEMT. Thus, our experiment consisted of membrane HEMTs with top-side passivation, double-side passivation, and a reference HEMT-on-Si. Mechanical probing support for the membrane-HEMTs was provided by filling the etched trenches with room-temperature-cure epoxy (EPO-TEK 301-2) [23].

DC and pulsed electrical measurements were performed using a Keithley 4200SCS parameter analyzer and a DiVA pulsed measurement system, respectively. Temperature-dependent characterization was performed inside a closed-loop He-cooled Lakeshore cryogenic probe station.

Thermal measurements were performed on a TMX Scientific T°Imager transient thermoreflectance (TR) imaging system with a 100X near-UV objective at 365 nm illumination wavelength, which is sufficient to render the AlGaN/GaN film opaque to the incident light and thus collect reflected light from within the first few nm of the AlGaN surface.[1] Details of the thermoreflectance method have been detailed elsewhere in [24]–[27]. The choice of the 365 nm illumination wavelength was based first on the knowledge of the bandgap of the III-Nitride material and then validated by a calibrated wavelength scan in the 330-450 nm range that confirmed an optimal TR response at the chosen wavelength. The measured change in reflectance ($\Delta R/R$) is proportional to the change in temperature as described by the known thermoreflectance relationship $\Delta T = (\Delta R/R)/C_{TR}$, where C_{TR} is the pixel-by-pixel calibrated coefficient of thermoreflectance. The specific calibrations performed on the devices in this work resulted in temperature measurements where 95% of the pixels were accurately measured to within 1 °C and most discarded pixels were edge regions adjacent to Au-overlay metal contacts. Broadband dark acquisition under bias showed that the electroluminescence (EL) signal had a negligible intensity of less than 0.1% of the thermoreflectance signal value. For the transient measurements, the gate was pulsed between −2.2 V and 0 V with either

1. The U.S. Navy does not endorse specific companies or products.

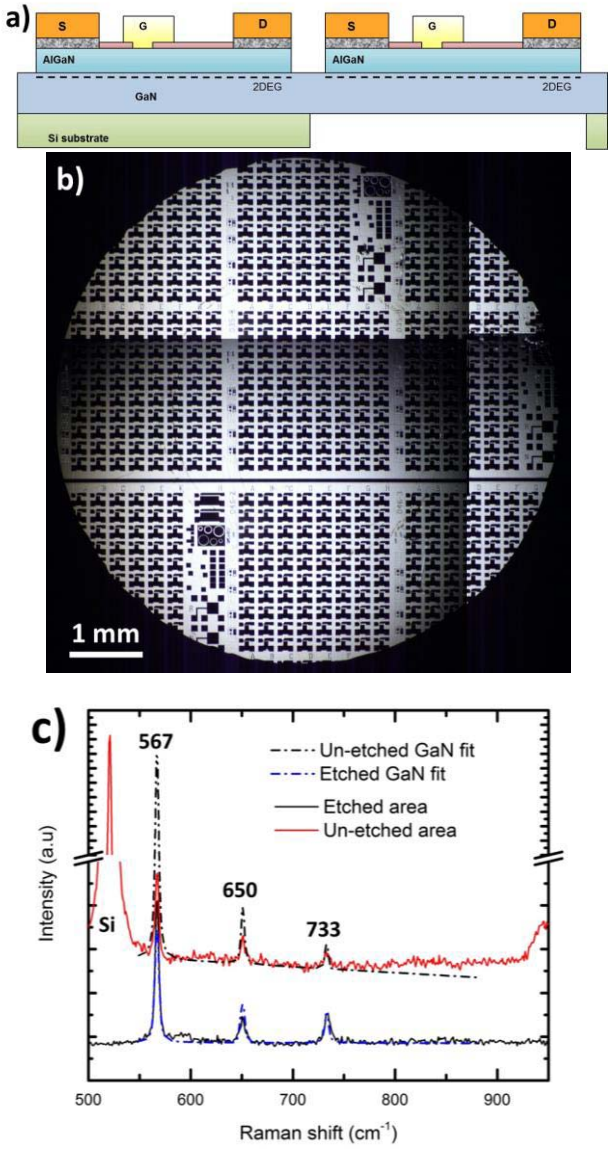

FIGURE 1. **a) Concept schematic, b) transmission-mode optical image, and c) measured and fitted Raman spectra of AlGaN/GaN membrane-HEMTs fabricated by selective etching of the Si substrate enabling same-die comparison of HEMTs with and without substrate.**

a sinusoidal or square bias, while a DC bias was applied on the drain contact.

III. ELECTRICAL CHARACTERIZATION

To quantify the effect of the Si etch on the resulting GaN HEMT membrane, Hall and Raman measurements were performed on a reference HEMT-on-Si and a membrane-HEMT with top-side SiN passivation, and the results are summarized in Table 1. The Hall measurements were limited to locations on the membrane where the Van der Pauw structures were present. The mobility was essentially unchanged, from 1520 $cm^2/V{\cdot}s$ off-membrane to 1562 $cm^2/V{\cdot}s$ measured on-membrane. A small increase in sheet carrier concentration of about 6% was measured, and was likely induced by increased biaxial strain in the absence of the substrate,

TABLE 1. **Property comparison for HEMT-on-Si and membrane-HEMTs.**

Property	HEMT-on-Si	Membrane-HEMT
R_{SH} (Ω/□)	678	621
μ_{HALL} ($cm^2/V{\cdot}s$)	1520	1562
N_{SH} (cm^{-2})	$6.06x10^{12}$	$6.44x10^{12}$
GaN E_2 (cm^{-1})	567.002 ± 0.067	567.02 ± 0.028
V_{BR} (V)	450	400

causing an increase in piezoelectric polarization field and thus a reduction in sheet resistance from 678 to 621 Ω/sq. This additional strain component, however, was not detected in the Raman data, measured on a HEMT mesa at the center of the membrane (Fig. 1c). The transverse-optical GaN E_2 peak position was fitted to 567 cm^{-1} in both cases, with a Si peak detectable only off-membrane. Optical microscopy also revealed that the heterostructure membrane did not buckle, which indicated that the membrane was not under compressive stress and was only under small tensile stress according to the Hall data. These observations agreed with prior reports of AlGaN/GaN membrane pressure sensors, where membrane deformation without applied pressure was not observed [11], [12].

Pulsed and static output characteristics comparing HEMT-on-Si and membrane-HEMTs are presented in Fig. 2. In both cases, a lower output drain current was measured on a membrane-HEMT. The ∼20% reduction in $I_{DSS,MAX}$, readily observable from the static membrane-HEMT measurements at $V_{DS} = 5$ V, indicated that self-heating effects resulted in much higher channel temperature in the absence of the Si substrate.

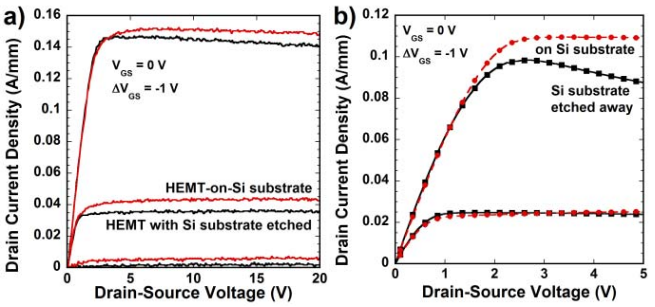

FIGURE 2. **a) Pulsed and b) static (DC) output characteristics (I_{DS}-V_{DS}) comparing HEMT-on-Si and Membrane-HEMT where the Si substrate was removed by wet etching.**

To further characterize membrane-HEMT DC performance, temperature dependent I_{DS}-V_{DS} and I_{DS}-V_{GS} curves were measured in the 12-300 K range, with only the 12 K and 300 K data shown in Fig. 3 for brevity. At 12 K, a maximum drain current of 0.35 A/mm was measured with 1 V gate bias, as well as peak transconductance of 0.15 S/mm at 1 V drain bias. The negative differential resistance at high drain bias, caused by self-heating, was observable at all temperatures and was particularly significant at 12 K. However, at that temperature and $V_{GS} = 0$ V, the saturation current

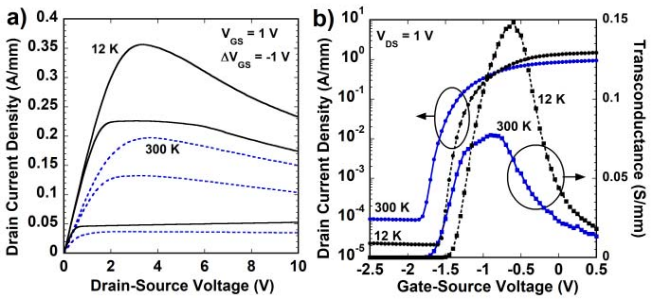

FIGURE 3. a) I_{DS}-V_{DS} and b) I_{DS}-V_{GS} (V_{DS} = 1 V) static characteristics of a typical membrane-HEMT at 12 K and 300 K temperature in vacuum.

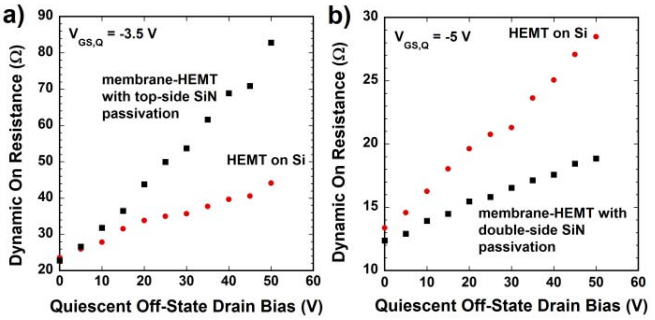

FIGURE 4. Dynamic on resistance as a function of off-state step stress comparing current collapse in membrane-HEMTs with a reference HEMT-on-Si for the case of a) top-side SiN passivation and b) double-side SiN passivation of the membrane-HEMT. A 100 nm thick SiN film was deposited in all cases.

plateaued at low drain bias before it started to decrease due to self-heating. This effect was less pronounced as the temperature increased and the onset of self-heating was expected to occur at lower output power levels. This delay in the onset of heating was also not observed at $V_{GS} = 1$ V, where the increase in output current caused the device to heat up as well. In addition, a slight increase in off-state drain current and a negative shift in threshold voltage were measured as the temperature increased towards 300 K (Fig. 3b) causing more electrically-active donor states in the heterostructure to become ionized [28].

Next, we compared the top-side and double-side SiN passivated membrane-HEMTs with the reference HEMT-on-Si. We note that SiN PECVD deposition on the N-polar side of the heterostructure resulted in about −1.5 V threshold voltage shift, the origin of which is not completely clear at present for the following reasons. First, SiN deposition inside the trench might have affected its stoichiometry, causing undesirable additional stress in that film. In addition, the PECVD process plasma might have created additional surface states on the already highly-defective N-polar AlGaN nucleation layers, causing an increase in net charged surface states on the back side of the HEMT. Furthermore, the higher conduction band of SiN (2.4 eV higher than Si) and lower electron affinity (2.1 eV, compared to 4.0 eV for Si) will also affect the charge distribution in the heterostructure and might contribute to the measurable shift in threshold voltage upon back-side SiN deposition. While separation of these effects is beyond the scope of this work, we emphasize that a SiN passivation process for N-polar nitrides would likely need significant process optimization in order to minimize undesirable surface effects caused by the process plasma.

The current collapse was quantified by measuring the increase in dynamic on resistance as a function of off-state step stress. The quiescent drain bias ($V_{DS,Q}$) was stepped from 0 to 50 V and the quiescent gate bias was constant ($V_{GS,Q} = V_{TH} - 2$ V) [29]. When the nucleation layers on the HEMT back side were not passivated (Fig. 4a), the dynamic on resistance at $V_{DS,Q} = 50$ V increased by nearly a factor of 2 relative to the reference HEMT-on-Si, corresponding to a 100% increase in current collapse. Conversely, a membrane-HEMT with double-side SiN passivation exhibited lower current collapse than the reference HEMT-on-Si, similarly by about a factor of 2, corresponding to 100 % improved current collapse. We expect this result to be improved even further with an optimized N-polar passivation process.

The last electrical characterization performed in this work compared the breakdown voltage of a membrane-HEMT and a HEMT-on-Si. The breakdown voltage measurement was performed in forward blocking mode at $V_{GS} = V_{TH} - 2$ V on a double-side passivated membrane-HEMT. The drain voltage was increased in 50 V increments and held steady for 60 seconds at each increment. This step-stress breakdown technique allowed the device to stabilize at each drain bias point, since a transistor under high field may become unstable and a linear increase in drain field would not allow the drain current to settle. An example of such recovery could be observed in Fig. 5 when the drain bias of the reference HEMT-on-Si was increased from 450 V to 500 V, where $I_{DS,OFF}$ settled before V_{DS} was increased again to 550 V, at which point the non-reversible breakdown event occurred.

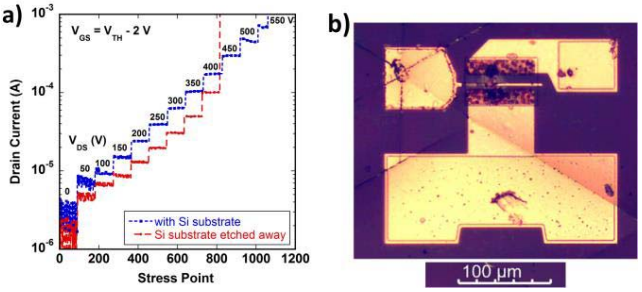

FIGURE 5. a) Off-state step stress comparison of HEMT-on-Si and Membrane-HEMT. V_{DS} was increased by 50 V every 100 s. b) Optical image of Membrane-HEMT upon catastrophic breakdown at V_{DS} = 400 V.

By comparison, the membrane-HEMT exhibited a lower off-state leakage current and also a lower breakdown voltage of 400 V. The hexagonally-oriented ruptures in the HEMT membrane responsible for the catastrophic failure during breakdown testing, pictured in Fig. 6, were similar to those observed during the temperature-dependent static

characterization. Such catastrophic failure could possibly be mitigated by avoiding the use of rigid probes during testing and potentially using low-force wirebonding to the membrane-HEMT.

IV. THERMAL CHARACTERIZATION

The removal of the Si substrate presented several challenges to the thermal characterization of the membrane-HEMTs. We expected a significant increase in device temperature and a corresponding heat induced motion (a.k.a., breathing) in both the device under test as well as the probes used during the test. The thermal chuck of the T°Imager system includes a piezoelectric stage (i.e., nanopositioner stage) that is primarily used for maintaining focus and position during calibration when the large temperature excursions produce appreciable thermal expansions. However, the nanopositioner is also useful for dynamically correcting the focus and position of the device under test during activation when self-heating produces local thermal expansions, as it did in the measurements reported on in this investigation.

Another significant concern for performing reliable thermoreflectance imaging of AlGaN/GaN HEMTs was the presence of electroluminescence under bias originating from defects in the III-Nitride films [30]. Such emission would present itself as an additive component to the measured change in surface reflectivity, thus potentially introducing significant error in the measurement. Therefore, dark spectra (no illumination) were initially collected using both a broadband and near-UV objective and under bias conditions representative of the ones used for subsequent thermal measurements. Under broadband collection, the measured intensity was about 0.17% of the thermoreflectance signal under 365 nm illumination. However, when using a near-UV sensitive objective (100x), the broadband emission typically observed in GaN in the yellow band was almost entirely filtered out; the collected intensity in this case was less than 0.01% of the measured TR signal, and could therefore be neglected.

Figure 6 presents a steady-state thermoreflectance map of a HEMT-on-Si adjacent to the membrane. The device was biased to yield up to 7.2 W/mm DC output power. For brevity, Fig. 6 shows comparable thermal maps for 1 and 3 W/mm (Fig. 6a-b), with a corresponding peak temperature of 83.5 °C at 3 W/mm. Figure 7a presents the temperature distribution in the channel up to 7.2 W/mm, where each temperature was calculated by averaging the measured pixels along the width of the device. As expected, the peak temperature occurs near the drain edge of the gate; however, we note that the peak temperature was measured about 0.5 μm away from the gate contacts towards the drain, likely due to localized heat spreading by the gate metal. A similar peak was observed near the source edge of the gate, however, a second peak also emerged as the power increased. The origin of the instability in the measured temperature at the source edge of the gate is not clear at this time and is subject to further investigation. Finally, we note that similar

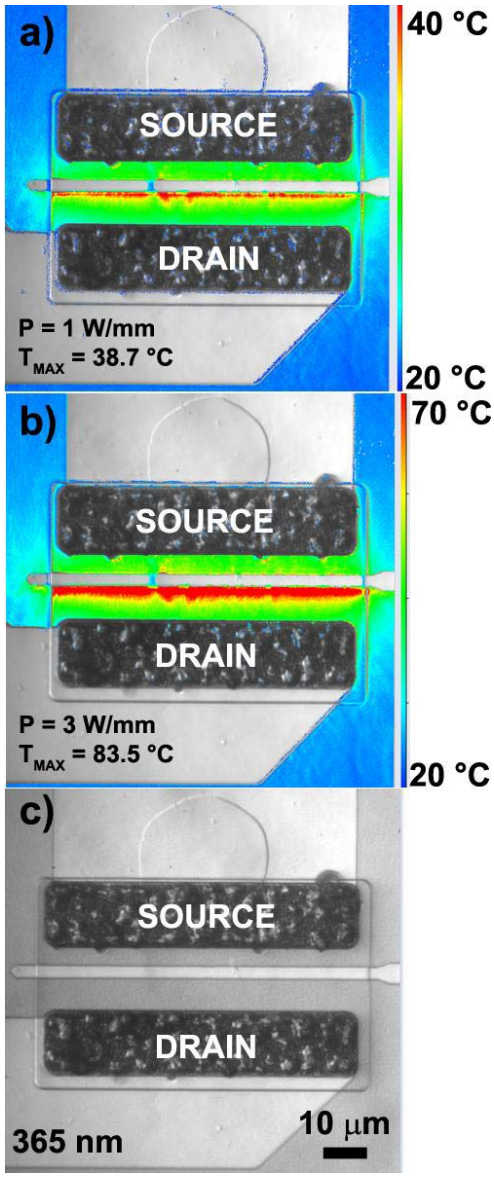

FIGURE 6. Steady state thermoreflectance maps of AlGaN/GaN HEMT-on-Si as a function of DC output power showing peak temperature in the gate-drain region of the HEMT at a) 1 W/mm and b) 3 W/mm. c) Optical image of the DUT acquired at 365 nm.

temperature levels were measured at the source and drain, independent of power (peak temperature).

By comparison, a membrane-HEMT activated at 1.1 W/mm yielded an average temperature of 180 °C near the drain edge of the gate (Fig. 7b), and only required 0.69 W/mm operating output power to reach a comparable peak temperature of a HEMT-on-Si biased at 7.2 W/mm. Thus, the absence of the Si substrate contributed about an order of magnitude decrease of steady-state power output of the device. Such a dramatic increase in temperature near the HEMT surface was accompanied by increased positional instability of the membrane relative to the objective, thus the error near the contacts (both sides of the gate) was higher than our tolerance threshold of one percent. Oscillations

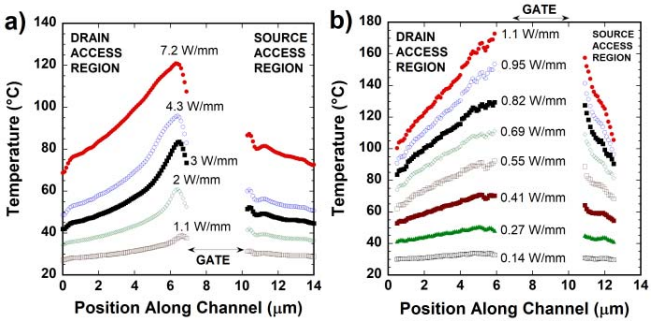

FIGURE 7. Temperature profiles as a function of position along source-drain channel and DC output power for a) HEMT-on-Si and b) membrane-HEMT measured by thermoreflectance imaging at 365 nm.

in the measured temperature near the gate at increasing power in Fig. 7b were observed from the membrane-HEMT, which was effectively subjected to accelerated aging in the absence of the thermomechanical support provided by the Si substrate.

Subsequent to the thermoreflectance mapping of the two devices in the steady state, transient TR maps were collected with a sinusoidal V_{GS} of 1 ms period and 2.2 V amplitude ($-2.2V \leq V_{GS} \leq 0V$) and a constant drain bias of $V_{DS} = 20$ V. Figures 8 presents the TR maps for the reference HEMT-on-Si and the membrane-HEMT, respectively, at t = 0 s ($V_{GS} = -2.2$ V), t = 0.25 ms, and t = 0.5 ms ($V_{GS} = 0$ V). In the off state, the reference HEMT did not exhibit any significant heating above baseplate temperature (Fig. 8a). On the other hand, the results in Fig. 8d indicate that the temperature on the HEMT membrane with the device biased in the off state reached a steady state value of about 45 °C at 1 W/mm, indicating that the time allowed by 1 ms pulse period was not sufficient for the membrane HEMT to cool back down to the baseplate temperature.

In the on state, owing to self-heating effects, a lower I_{DS} was measured for the membrane-HEMT, resulting in output power of about 1 W/mm, compared to 1.63 W/mm for the HEMT-on-Si at the maximum gate bias (Fig. 8f and 8c, respectively). The membrane-HEMT exhibited average temperatures of 113.9-114.7 °C in the channel region at peak V_{GS} (Fig. 8f), with less than 1 °C difference in temperature measured between the source and the drain regions, which is attributed to be within the accuracy of the TR measurement (0.87% difference). The reference HEMT-on-Si, on the other hand, exhibited a peak temperature of just 34 °C at 1.63 W/mm, more than a factor of 3 lower, with the temperature returning to the baseplate value of 20 °C within a few micrometers away from the mesa region (Fig. 8c).

To determine the heating and cooling rates for the two HEMTs, square pulses of 2.2 V amplitude (-2.2 V $\leq V_{GS} \leq 0$) and 1 ms period were applied to the gate with a 20 % duty cycle and a –30 % phase shift (corresponding to a 0.3 ms delay from the beginning of the pulse period to the V_{GS} pulse edge in Fig. 10). The results are presented in Fig. 9 as a function of DC power for the

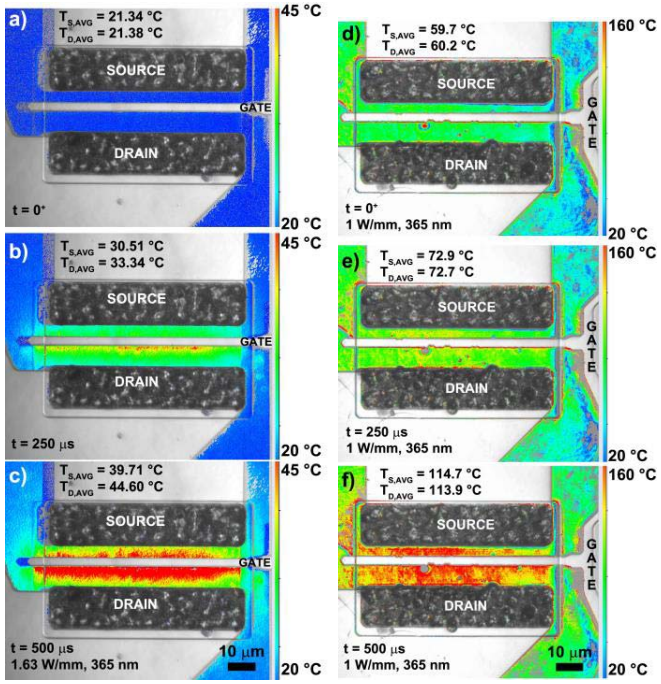

FIGURE 8. Transient thermoreflectance maps of a-c) AlGaN/GaN HEMT-on-Si and d-f) AlGaN/GaN Membrane-HEMT under sinusoidal V_{GS} operation ($-2.2 = V_{GS} = 0$ V) with 1 ms period and $V_{DS} = 20$ V. Averaged temperature in the G-S and G-D access regions shown at a,d) t = 0 μs, b,e) t = 250 μs, and c,f) t = 500 μs.

reference and membrane-HEMTs, respectively. Once again, reduction in drain current caused the membrane-HEMT to exhibit lower output power at identical drain bias. In both cases, the peak measured temperature values at t = 400 μs are reported. At about 2.96 W/mm, the reference HEMT exhibited a somewhat surprisingly low channel temperature (53.74 °C), with a time-dependent distribution shown in Fig. 10a for each of the three bias conditions. On the other hand, at 1.9 W/mm the temperature of the membrane-HEMT measured under square-pulse transient operation reached a peak value of 148.5 °C for the case of 1.9 W/mm output power. The time-dependence of the measured temperatures (Fig. 10b) suggested that the 50 μs time step between measurements was sufficient to capture the exponential decrease in temperature in the membrane-HEMT.

The exponential decrease in temperature upon turning off the gate bias in the membrane-HEMT was fit with a single-exponential term function with good agreement (Fig. 11), indicating that the assumption of lateral heat flow in the membrane-HEMT appears to be valid. From the exponential fit to the temperature decay, a time constant of 66.7 μs was calculated at 1.9 W/mm output power. Kuball *et al.* [18] employed a similar exponential fit to calculate time constants for vertical heat flow in AlGaN/GaN HEMTs on sapphire and SiC. Their data suggested that lateral heat flow in the device was clearly present and should be accounted for by incorporating a sum of exponential functions. In our case, due to the absence of a thermally conductive substrate, a single exponential term was sufficient

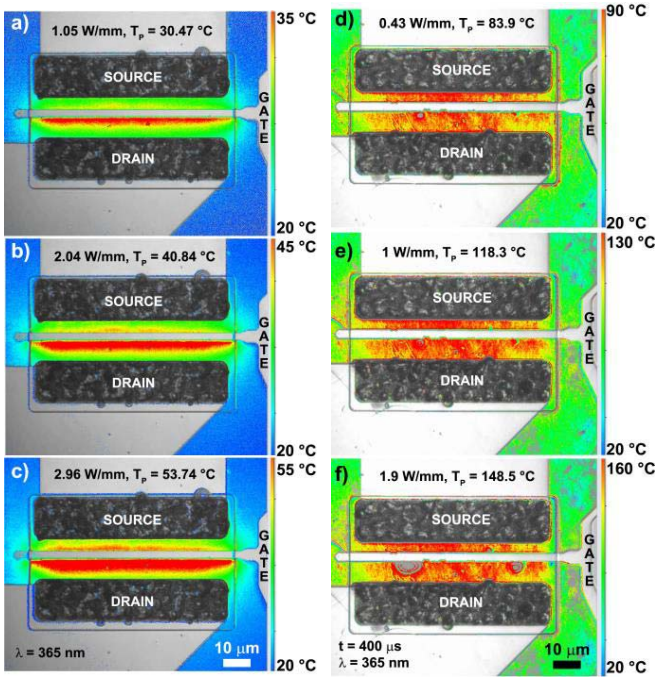

FIGURE 9. Transient thermoreflectance maps of a-c) AlGaN/GaN HEMT-on-Si and d-f) AlGaN/GaN Membrane-HEMT under square V_{GS} pulse operation ($-2.2 = V_{GS} = 0$ V) with 1 ms period and 20 % duty cycle as a function of DC output power. Peak temperature in the G-D access region shown at a) 1.05 W/mm, b) 2.04 W/mm, c) 2.96 W/mm, d) 0.43 W/mm, e) 1 W/mm, and f) 1.9 W/mm at t = 400 μs.

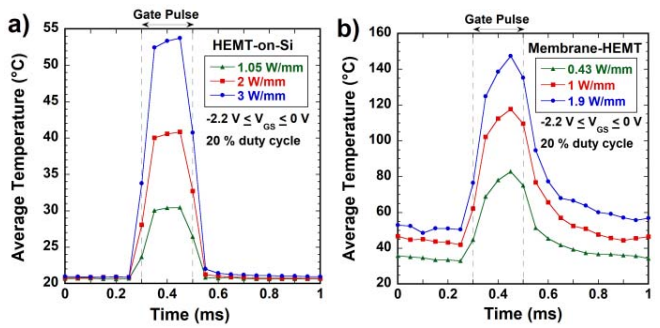

FIGURE 10. Average temperature on a) AlGaN/GaN HEMT-on-Si and b) Membrane-HEMT as a function of DC output power and using a square-pulse gate bias ($-2.2 = V_{GS} = 0$ V, 1 ms period, 20% duty cycle) measured by transient thermoreflectance at 50 μs intervals using a 365 nm LED source.

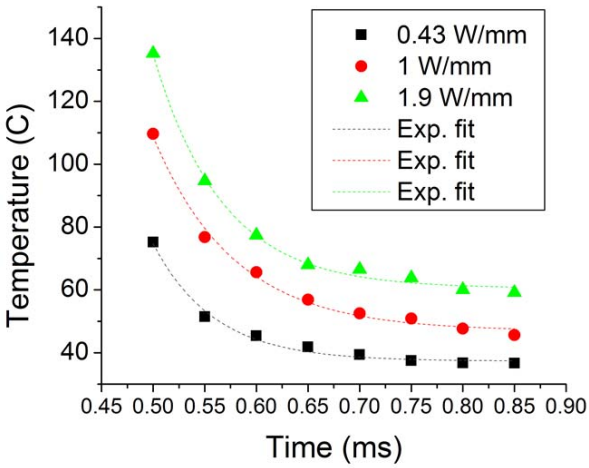

FIGURE 11. Single-exponential fit of the temperature data from Fig. 10b during cool-down regime after V_{GS} pulsed applied to the membrane-HEMT returned to $V_{GS} = -2.2$ V at t = 500 μs.

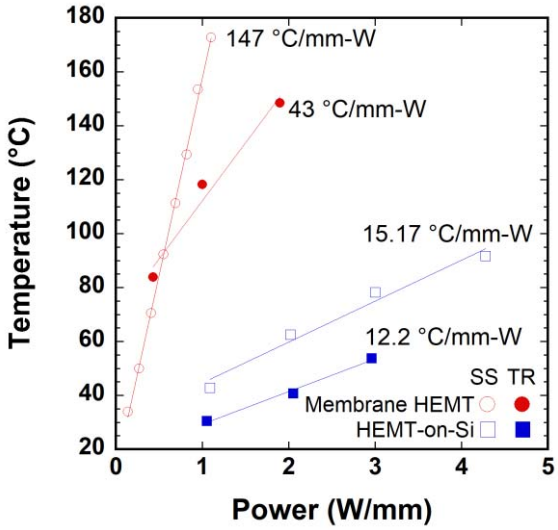

FIGURE 12. Comparison of peak temperature as a function of DC output power for Membrane-HEMT and HEMT-on-Si, measured by both steady state and transient thermoreflectance. Thermal resistances extracted from the slope of each curve is indicated for both the steady state and transient measurement.

to describe heat flow in the membrane, and the measured time constant values (59 μs to 78 μs, depending on bias) were all significantly higher than the 10 μs experimental value reported by Kuball for vertical heat flow for HEMTs on SiC.

Finally, the thermal resistance of the HEMT-on-Si and the membrane-HEMT were compared as a function of output power during both steady-state and transient TR (Fig. 12). A thermal resistance of 144 and 43 °C/mm-W was obtained using steady-state and transient conditions, respectively, for the membrane-HEMT from a linear fit of the data. These values for thermal resistance did not exclude the contribution of the epoxy and the SiN passivation layers, which was minimal as their thermal conductivity was very low. Significantly lower thermal resistance was obtained for the reference HEMT-on-Si, where the 12.2 °C/mm-W obtained under transient conditions approached the 15.17 °C/mm-W in steady state. We note that these thermal resistances were calculated using temperature values measured near the HEMT surface and averaged in the gate-drain access region (excluding pixels near metal and mesa edges), as opposed to the thermal resistance of a HEMT-on-Si obtained from the Raman peak of the Si substrate (3.6 °C/mm-W) [3]. These values were thus consistently higher than thermal resistances for HEMTs on Si and SiC reported using steady-state Micro-Raman spectroscopy [31], [32].

V. CONCLUSION

In summary, we have quantified for the first time the electrothermal performance of an AlGaN/GaN HEMT membrane, where the substrate was removed without damaging the N-polar side of the heterostructure. Thermoreflectance imaging shows with convincing accuracy that self-heating will significantly increase device temperature during operation even at very low power; nevertheless, almost 2 W/mm operation of a membrane-HEMT was demonstrated. We also show that removing the Si substrate with a wet etch does not necessarily degrade the electrical characteristics of the HEMT, as evidenced by Raman and Hall measurements. The double-side SiN passivated membrane-HEMT showed improved current collapse and lower off-state leakage current, suggesting that membrane-HEMTs can exhibit good performance as long as their operating power is kept within safe thermal operating constraints.

APPENDIX

Supplemental transient thermoreflectance video of AlGaN/GaN HEMTs available online.

ACKNOWLEDGMENT

The authors are sincerely grateful to Travis L. Sandy and Johanna H. Reimer (both of TMX Scientific) for thermoreflectance measurements and system support, Dr. Laura Ruppalt, Dr. James Champlain, and Dr. Mario Ancona (NRL) for preliminary TR/IR measurements, modeling, and useful discussions, as well as the NRL Nanoscience Institute (Dean St. Amand, Walter Spratt, Dr. Anthony Boyd) for fabrication equipment support. Research at NRL was supported by the Office of Naval Research.

REFERENCES

[1] A. Krost and A. Dadgar, "GaN-based devices on Si," *Physica Status Solidi (A)*, vol. 194, no. 2, pp. 361–375, 2002, doi: 10.1002/1521-396X(200212)194:2<361::AID-PSSA361>3.0.CO;2-R.

[2] E. M. Chumbes *et al.*, "AlGaN/GaN high electron mobility transistors on Si(111) substrates," *IEEE Trans. Electron Devices*, vol. 48, no. 3, pp. 420–426, Mar. 2001, doi: 10.1109/16.906430.

[3] M. J. Tadjer *et al.*, "Reduced self-heating in AlGaN/GaN HEMTs using nanocrystalline diamond heat-spreading films," *IEEE Electron Device Lett.*, vol. 33, no. 1, pp. 23–25, Jan. 2012, doi: 10.1109/LED.2011.2171031.

[4] T. J. Anderson *et al.*, "Improved GaN-based HEMT performance by nanocrystalline diamond capping," in *Device Res. Conf. Dig.*, 2012, pp. 155–156, doi: 10.1109/DRC.2012.6256985.

[5] P. Srivastava *et al.*, "Record breakdown voltage (2200 V) of GaN DHFETs on Si with 2-μm buffer thickness by local substrate removal," *IEEE Electron Device Lett.*, vol. 32, no. 1, pp. 30–32, Jan. 2011, doi: 10.1109/LED.2010.2089493.

[6] N. Herbecq *et al.*, "1900 V, 1.6 mΩ cm^2 AlN/GaN-on-Si power devices realized by local substrate removal," *Appl. Phys. Exp.*, vol. 7, no. 3, 2014, Art. no. 034103, doi: 10.7567/APEX.7.034103.

[7] B. Lu and T. Palacios, "High breakdown (> 1500 V) AlGaN/GaN HEMTs by substrate-transfer technology," *IEEE Electron Device Lett.*, vol. 31, no. 9, pp. 951–953, Sep. 2010, doi: 10.1109/LED.2010.2052587.

[8] M. Azize and T. Palacios, "Effect of substrate-induced strain in the transport properties of AlGaN/GaN heterostructures," *J. Appl. Phys.*, vol. 108, no. 2, 2010, Art. no. 023707, doi: 10.1063/1.3463150.

[9] M. J. Tadjer *et al.*, "Characterization of strained AlGaN/GaN HEMTs on CMP-thinned Si substrates," in *CS Mantech Conf. Dig.*, 2015, pp. 115–118. [Online]. Available: http://csmantech.org/OldSite/Digests/2015/papers/6.3-033.pdf

[10] B. S. Kang *et al.*, "Capacitance pressure sensor based on GaN high-electron-mobility-transistor-on-Si membrane," *Appl. Phys. Lett.*, vol. 86, no. 25, 2005, Art. no. 253502, doi: 10.1063/1.1952568.

[11] B. S. Kang *et al.*, "Pressure-induced changes in conductivity of AlGaN/GaN high-electron-mobility transistor membranes," *Appl. Phys. Lett.*, vol. 85, no. 14, p. 2962, 2004, doi: 10.1063/1.1800282.

[12] T. Lalinsky *et al.*, "Micromachined membrane structures for pressure sensors based on AlGaN/GaN circular HEMT sensing device," *Microelectron. Eng.*, vol. 98, pp. 578–581, Oct. 2012, doi: 10.1016/j.mee.2012.06.014.

[13] T.-H. Chang *et al.*, "Strain balanced AlGaN/GaN/AlGaN nanomembrane HEMTs," *Sci. Rep.*, vol. 6, p. 6360, Jul. 2017, doi: 10.1038/s41598-017-06957-8.

[14] S. Mhedhbi *et al.*, "Recent improvements in flexible GaN-based HEMT technology," *Physica Status Solidi (A)*, vol. 214, no. 4, 2017, Art. no. 1600484, doi: 10.1002/pssa.201600484.

[15] D. J. Meyer *et al.*, "Epitaxial lift-off and transfer of III-N materials and devices from SiC substrates," *IEEE Trans. Semicond. Manuf.*, vol. 29, no. 4, pp. 384–389, Nov. 2016, doi: 10.1109/TSM.2016.2599839.

[16] M. J. Tadjer *et al.*, "Quantifying substrate removal induced electrothermal degradation in AlGaN/GaN HEMTs," in *Proc. Device Res. Conf.*, 2017, pp. 1–2, doi: 10.1109/DRC.2017.7999411.

[17] M. G. Ancona, S. C. Binari, and D. J. Meyer, "Fully coupled thermo-electromechanical analysis of GaN high electron mobility transistor degradation," *J. Appl. Phys.*, vol. 111, no. 7, 2012, Art. no. 074504, doi: 10.1063/1.3698492.

[18] M. Kuball *et al.*, "Time-resolved temperature measurement of AlGaN/GaN electronic devices using micro-Raman spectroscopy," *IEEE Electron Device Lett.*, vol. 28, no. 2, pp. 86–89, Feb. 2007, doi: 10.1109/LED.2006.889215.

[19] S. Martin-Horcajo *et al.*, "Transient thermoreflectance for gate temperature assessment in pulse operated GaN-based HEMTs," *IEEE Electron Device Lett.*, vol. 37, no. 9, pp. 1197–1200, Sep. 2016, doi: 10.1109/LED.2016.2595400.

[20] J. Kuzmík *et al.*, "Transient thermal characterization of AlGaN/GaN HEMTs grown on silicon," *IEEE Electron Device Lett.*, vol. 52, no. 8, pp. 1698–1705, Aug. 2005, doi: 10.1109/TED.2005.852172.

[21] K. Maize *et al.*, "High resolution thermal characterization and simulation of power AlGaN/GaN HEMTs using micro-Raman thermography and 800 picosecond transient thermoreflectance imaging," in *Proc. IEEE Compd. Semicond. Integr. Circuit Symp. (CSICS)*, 2014, pp. 1–8, doi: 10.1109/CSICS.2014.6978561.

[22] B. Schwartz and H. Robbins, "Chemical etching of silicon," *J. Electrochem. Soc.*, vol. 123, no. 12, pp. 1903–1909, 1976.

[23] *Datasheet*. Accessed: Jul. 25, 2016. [Online]. Available: http://www.epotek.com

[24] M. Farzaneh *et al.*, "CCD-based thermoreflectance microscopy: Principles and applications," *J. Phys. D Appl. Phys.*, vol. 42, no. 14, 2009, Art. no. 143001, doi: 10.1088/0022-3727/42/14/143001.

[25] M. G. Burzo, P. L. Komarov, and P. E. Raad, "Noncontact transient temperature mapping of active electronic devices using the thermoreflectance method," *IEEE Trans. Compon. Packag. Manuf. Technol.*, vol. 28, no. 4, pp. 637–643, Dec. 2005, doi: 10.1109/TCAPT.2005.859738.

[26] P. E. Raad, P. L. Komarov, and M. G. Burzo, "An integrated experimental and computational system for the thermal characterization of complex three-dimensional submicron electronic devices," *IEEE Trans. Compon. Packag. Manuf. Technol.*, vol. 30, no. 4, pp. 597–603, Dec. 2007, doi: 10.1109/TCAPT.2007.910043.

[27] P. E. Raad, P. L. Komarov, and M. G. Burzo, "Thermal characterization of embedded electronic features by an integrated system of CCD thermography and self-adaptive numerical modeling," *Microelectron. J.*, vol. 39, no. 7, pp. 1008–1015, 2008, doi: 10.1016/j.mejo.2007.11.006.

[28] Y. Cai, Y. Zhou, K. M. Lau, and K. J. Chen, "Control of threshold voltage of AlGaN/GaN HEMTs by fluoride-based plasma treatment: From depletion mode to enhancement mode," *IEEE Trans. Electron Dev.*, vol. 53, no. 9, pp. 2207–2215, Sep. 2006, doi: 10.1109/TED.2006.881054.

[29] M. J. Tadjer *et al.*, "A tri-layer PECVD SiN passivation process for improved AlGaN/GaN HEMT performance," *ECS J. Solid State Sci. Technol.*, vol. 6, no. 1, pp. P58–P61, 2017, doi: 10.1149/2.0231701jss.
[30] M. J. Tadjer *et al.*, "Electrical and optical characterization of AlGaN/GaN HEMTs with in situ and ex situ deposited SiN layers," *J. Elect. Mater.*, vol. 39, no. 11, pp. 2452–2458, 2010, doi: 10.1007/s11664-010-1343-9.
[31] M. Kuball *et al.*, "Measurement of temperature distribution in multifinger AlGaN/GaN heterostructure field-effect transistors using micro-Raman spectroscopy," *Appl. Phys. Lett.*, vol. 82, no. 1, p. 124, 2003, doi: 10.1063/1.1534935.
[32] G. Pavlidis, D. Mele, T. Cheng, F. Medjdoub, and S. Graham, "The thermal effects of substrate removal on GaN HEMTs using Raman thermometry," in *Proc. 15th Intersoc. Conf. Ther. Thermomech. Phenom. Elect. Syst. (ITherm)*, 2016, pp. 1255–1260. doi: 10.1109/ITHERM.2016.7517691.

MARKO J. TADJER received the undergraduate degree in electrical and computer engineering from the University of Arkansas in 2002, the Master of Science degree in electrical engineering from Duke University in 2004, and the Ph.D. degree in electrical engineering from the University of Maryland, College Park, in 2010. He is an Electronics Engineering Civilian Research Scientist with the U.S. Naval Research Laboratory, Washington, DC, USA. He has completed postdoctoral fellowships with the Technical University of Madrid in 2013 and at the Power Electronics Branch of the U.S. Naval Research Laboratory. His research in III-Nitride, III-Oxide, and SiC power devices focuses on the integration of materials with attractive properties such as diamond, graphene, and novel dielectrics. He has authored or co-authored over 150 archival publications, over 200 conference presentations, as well as 11 issued U.S. patents and 1 book chapter. He was a recipient of the Karles' Fellowship in 2015.

PETER E. RAAD received the B.S.M.E. (Hons.), M.S., and Ph.D. degrees in mechanical engineering from the University of Tennessee, Knoxville, in 1980, 1981, and 1986, respectively. He is a Professor of mechanical engineering with Southern Methodist University (SMU), Dallas, TX, USA. He first joined SMU in 1986, where he has served as the Associate Dean with the School of Engineering. From 2000 to 2012, he founded and directed the Hart eCenter with SMU, a university-wide center to address the impact of the interactive networked technologies on society. He also founded and directed the Guildhall with SMU, a first of its kind, graduate program in digital game development. He has received over $2.5 million in funding support for his research in tsunami mitigation and in metrology of submicron electronics. In 2006, he founded TMX Scientific, a company to innovate and commercialize deep submicron thermal measurement systems and ultrafast thermal computational engines. His work in the thermal management field includes the development of innovative deep-submicron thermal metrology techniques and systems, as well as novel coupling of computations and measurements to provide transient, 3-D temperature fields in electronic structures with inaccessible internal features. He has published over 50 journal articles and given over 100 conference and invited talks. He holds U.S. and international patents in thermal metrology and computational characterization of multiscale integrated circuits. He was a recipient of the Allan Kraus Thermal Management Medal in 2014, the Harvey Rosten Award for Excellence in the Physical Design of Electronics in 2006, the ASME North Texas Section Engineer of the Year 1999–2000, the Next-Gen's Top 25 People of 2007 (most influential in the video gaming industry), and the Outstanding Graduate (four times) and Undergraduate (three times) Faculty Awards at SMU. He is a fellow of ASME.

PAVEL L. KOMAROV received the Ph.D. degree in physics and mathematics from the Institute for High Temperatures, Russian Academy of Sciences in 1996. He joined the Nanoscale Electro-Thermal Sciences Laboratory with SMU in 1997, where he has been a Lead Designer and a Developer of experimental and numerical tools for the thermal measurements of thin-film materials and micro-electronic devices. He is currently the Director of Technology with TMX Scientific Company, which has been started on the base of SMU NETSL Laboratory in 2007. He has published over 45 articles. He was a recipient of the Harvey Rosten Award for Excellence in 2006.

KARL D. HOBART received the B.S. degree in physics from the University of Illinois in 1984 and the M.S. and Ph.D. degrees in electrical engineering from the University of Delaware in 1987 and 1990, respectively. He was a Post-Doctoral Fellow with the Naval Research Laboratory (NRL) concentrated on molecular beam epitaxy of silicon and germanium alloys and material characterization. In 1993, he joined the Microelectronics Device Physics Section with NRL, where he led a successful effort on the growth, fabrication, and characterization of microwave power SiGe heterojunction transistors. He presently heads the High Power Devices Section with the High Power Electronics Branch, NRL. His research interests include wide bandgap power electronics for high voltage and high frequency applications, diamond integration for thermal management, and wafer bonding technology. He has authored or co-authored over 180 technical articles and holds 39 patents.

TATYANA I. FEYGELSON has 20 years of experience in material science and engineering, and over 60 publications. Her area of expertise includes diamond chemical vapor deposition, and material analysis and integration.

ANDREW D. KOEHLER received the B.S., M.S., and Ph.D. degrees in electrical engineering from the University of Florida in 2004, 2006, and 2011, respectively. He is an Electronics Engineering Civilian Research Scientist with the U.S. Naval Research Laboratory (NRL), Washington, DC, USA. In 2012, he joined the High Power Electronics Branch, Electronic Science and Technology Division, NRL. The focus of his current research includes power device design, fabrication, characterization, radiation effects on GaN high electron mobility transistors (HEMTs), thermal management of high power GaN HEMTs, graphene base hot electron transistors for THz applications, vertical GaN power devices, and device failure mechanisms and physics.

TRAVIS J. ANDERSON received the B.S. degree in chemical engineering from the Georgia Institute of Technology in 2004 and the Ph.D. degree in chemical engineering from the University of Florida in 2008. He is a Civilian Staff Scientist with the U.S. Naval Research Laboratory.

ANINDYA NATH received the B.Tech. degree from the West Bengal University of Technology and the Ph.D. degree in electrical engineering from George Mason University in 2014. He joined the Department of Science and Technology, Jadavpur University, India, as a Research Scholar. He joined the U.S. Naval Research Laboratory, Washington, DC, USA, as a Residence Post-Doctoral Associate. He joined GlobalFoundries as a Senior Quality Engineer in 2017, where he is currently working on 7-nm Si-Ge Fin-based technology.

BRADFORD PATE received the Ph.D. degree in applied physics from Stanford University in 1984. His research interests center on electronic and mechanical properties of diamond materials. He is a Research Physicist with the Chemistry Division, U.S. Naval Research Laboratory.

FRITZ J. KUB (F'11) received the B.S. degree in engineering physics from South Dakota State University in 1972, the M.S. degree in electrical engineering from the University of Minnesota in 1976, and the Ph.D. degree in electrical engineering from the University of Maryland in 1985. He is currently the Head of the Power Electronics Branch, Naval Research Laboratory. He has over 220 journal publications and 74 U.S. patents. He was a recipient of two Naval Research Laboratory Best Publication Awards, the Naval Research Laboratory Edison Award, five Naval Research Laboratory Technology Transfer Awards, the University of Maryland Innovation Hall of Fame Award in 2014, and the Distinguished Engineer Award from South Dakota State University in 2010.